Bull. Korean Chem. Soc. 2014, Vol. 35, No. 5 1349
http://dx.doi.org/10.5012/bkcs.2014.35.5.1349

Facile Synthesis of Co_3O_4/Mildly Oxidized Multiwalled Carbon Nanotubes/Reduced Mildly Oxidized Graphene Oxide Ternary Composite as the Material for Supercapacitors

Mei-yu Lv, Kai-yu Liu,* Yan Li, Lai Wei, Jian-jian Zhong, and Geng Su†,*

School of Chemistry and Chemical Engineering, Central South University, Changsha 410083, P.R. China
**E-mail: kaiyuliu@263.net*
*†College of Material Science and Engineering, Central South University of Forestry and Technology, Changsha 410004, China. *E-mail: sugeng1996@126.com*
Received November 22, 2013, Accepted January 10, 2014

A three-dimensional (3D) Co_3O_4/mildly oxidized multiwalled carbon nanotubes (moCNTs)/reduced mildly oxidized graphene oxide (rmGO) ternary composite was prepared *via* a simple and green hydrolysis-hydrothermal approach by mixing $Co(Ac)_2\cdot 4H_2O$ with moCNTs and mGO suspension in mixed ethanol/H_2O. As characterized by scanning electron microscopy and transmission electron microscopy, Co_3O_4 nanoparticles with size of 20-100 nm and moCNTs are effectively anchored in mGO. Cyclic voltammetry and galvanostatic charge-discharge measurements were adopted to investigate the electrochemical properties of Co_3O_4/moCNTs/rmGO ternary composite in 6 M KOH solution. In a potential window of 0-0.6 V *vs*. Hg/HgO, the composite delivers an initial specific capacitance of 492 F g^{-1} at 0.5 A g^{-1} and the capacitance remains 592 F g^{-1} after 2000 cycles, while the pure Co_3O_4 shows obviously capacitance fading, indicating that rmGO and moCNTs greatly enhance the electrochemical performance of Co_3O_4.

Key Words : Cobalt oxide nanoparticles, Mildly oxidized Graphene, Mildly oxidized multiwalled carbon nanotubes, Hydrothermal method, Supercapacitors

Introduction

One of the great challenges for today's information-rich, mobile society is providing high-efficient, low-cost, and environmentally friendly electrochemical energy conversion and storage devices for powering an increasingly diverse range of applications, ranging from portable electronics to electric vehicles (EVs) or hybrid EVS (HEVs).[1,2] As the performance of these devices depends intimately on the properties of their materials, considerable attention has been paid to the research and development of key materials.[3-10] Supercapacitors (also known as electrochemical capacitors or ultracapacitors) have drawn tremendous attention as an energy storage device for their high power density, good rate performance and long cycling life. They are playing an increasingly important role in various applications ranging from portable electronics to hybrid electric vehicles.[11] They are usually defined into electrochemical double layer capacitors (EDLCs) and pseudo-capacitors based on their different energy storage mechanisms.

Generally, the carbon and carbon nanotubes (CNTs) with high surface area and readily accessible mesopores are widely used for EDLCs, where the charge storage process is non-Faradic and energy storage is electrostatic.[12] Graphene, which is a flat monolayer of carbon atoms tightly packed into a two-dimensional (2D) honeycomb lattice,[13] has emerged as a promising material for electrochemical energy storage applications owing to its various superiorities in mechanical, electronic (with carrier mobility up to 200 000 $cm^2\ V^{-1}\ s^{-1}$),[14,15] thermal conductivity (~4840-5300 W m^{-1} K^{-1}),[15] elasticity,[16] and specific surface area (~2600 $m^2\ g^{-1}$).[17] At the same time, the capacitance of the pseudo-capacitors is mainly from Faradic redox reaction. Their electrode materials generally involve various metal oxides[18-22] and conductive polymers.[23-30] In recent years, transition metal oxides have been drawn extensive research attentions for pseudo-capacitors since they could provide higher capacitance than carbon materials and longer cycling life than conductive polymers.[31-33] Among these materials, Co_3O_4 shows an inviting prospect because of its ultra-high theoretical specific capacitance of 3560 F g^{-1}. Also, Co_3O_4 is one of the most promising electrode materials for commercial supercapacitors due to their good efficiency, better stability, high abundance, low cost, environmental benignity, and relatively broad work potential window in aqueous solution. However, the poor electronic conductivity of Co_3O_4 has hindered its further application for high-power electrochemical capacitor. Thus, it is of great importance to employ effective strategies to enhance the electronic conductivity of Co_3O_4 and maintain high electrolyte penetration diffusion rates with the aim of improving its electrochemical capacitive performance. The common approach is either embedding Co_3O_4 nanoparticles into or depositing Co_3O_4 nanoparticles on a highly conductive porous matrix to form composites. To date, many Co_3O_4/carbon composites systems have been investigated for supercapacitor application. But all of these results are far from meeting the needs of commercial application due to their complexity in synthesis, relatively low capacitance, or insufficient stability. Thus, the facile synthesis of Co_3O_4 composite with better electrochemical performance is still a hot issue to address. Currently, graphene/metal oxide composites are drawing increasing attention as electrode materials since the ultrathin flexible graphene sheets can provide a support to anchor metal oxide nanoparticles and serve as a highly conductive matrix.[34-35] There are many studies of graphene based composites such as graphene/MnO_2 (315 F g^{-1} in 1 M Na_2SO_4),[36] graphene/Co_3O_4 (548 F g^{-1} in 6 M KOH).[37] But the complicated synthesis processes greatly limited its commercial application. Graphene composites *via* one-step solvothermal process exhibited a specific capacitance of 147 F g^{-1}.[38] Myoungho Pyo *et al.* also reported that the SnO_2-anchored graphene was subjected to thermal reduction in order to enhance the crystallinity of SnO_2 and the electrochemical conductivity of graphene.[39,40] Noting that the utilization of toxic and oxidative dimethyl sulfoxide (DMSO) as solvent made it environmentally unfriendly and probably could result in incomplete reduction of graphite oxide to graphene.

Consequently, it is still a big challenge to develop a facile simple and rapid approach to synthesize better performance Co_3O_4/graphene composites. It is known that the electrochemical properties of the composites greatly depend on the structural features of graphene and the degree of homogenous dispersion. Herein, Co_3O_4 nanoparticles are homogeneously embedded into the graphene nanosheets *via* a simple solvothermal process which does not require the reduction of graphite oxide to graphene at first and no any toxic organic solvent is used.

Experimental

Chemicals. Multiwalled carbon nanotubes with 40–60 nm in diameter and 5–15 μm in length were purchased from Shenzhen Nanotech Port Co. Ltd. Cobalt acetate [$Co(CH_3COO)_2\cdot 4H_2O$], $KMnO_4$, $NaNO_3$, H_2O_2 were purchased from Sinopharm Chemical Reagent (Co., Ltd). All chemicals were used as received from vendors without further purification. Deionized water was prepared in our laboratory.

Material Synthesis and Characterization. The mildly oxidized CNTs (moCNT) were made by a modified Hummer's method.[41] Mildly oxidized graphene oxide (mGO) was made from flake graphite (200 mesh) by a modified Hummer's method[42] using a lower concentration of oxidizing agent. Typically, as-prepared mGO sample was dissolved in an aqueous solution (0.8 mg/mL). For the first step synthesis of hybrid, 62.5 mL of mGO aqueous solution was ultrasonicated for 2 h. Then 12.5 mL of 0.24 M $Co(Ac)_2$ aqueous solution was added to 200 mL of moCNT (25 mg) ethyl alcohol suspension by ultrasonic agitation for 2 h. The mixture solution was then dropped into the mGO aqueous solution. The reaction was kept at 80 °C under magnetic stirring for 8 h. Another 475 mL of anhydrous ethanol was added to the mixed solution four times in every two hours. In the first step, Co_3O_4 nanoparticles and moCNTs were grown on mildly oxidized GO sheets (mGO) freely suspended in solution by hydrolysis and oxidation of cobalt acetate. After that, the reaction mixture from the first step was transferred to a 100 mL autoclave for hydrothermal reaction at 150 °C for 8 h. This subsequent hydrothermal step also led to form crystallization of Co_3O_4 and reduction of mGO to form the Co_3O_4/moCNTs/rmGO hybrid. The resulted product was collected by vacuum filtration and washed by deionized water 3 times and anhydrous ethanol 3 times. The resulting hybrid was ~150 mg after lyophilization.

The crystal structures of samples were determined by X-ray diffractometer (XRD, Rigaku D/max 2550VB$^+$) from 10° to 80° with Cu Kα radiation (λ = 1.54056 Å). The Fourier transform infrared (FT-IR) spectra were recorded on Nicolet 560 spectroscopy with KBr pellet technique. Thermal-gravimetric analysis was carried out on NETZSCH STA449C thermalanalyzer under air atmosphere at temperature ranging from 30 °C to 900 °C with a heating rate of 10 °C min^{-1}. Raman spectra were tested with Dior LABRAM-1B instrument. The surface morphology was characterized by scanning electron microscope (SEM; JEOL JSM-6360 LV), transmission electron microscope (TEM; JEOL JEM-2100 F) and high-resolution transmission electron microscopy (HRTEM, JEOL-2010) at an acceleration voltage of 200 kV.

Electrode Preparation and Electrochemical Analysis. The working electrode was prepared by mixing 85 wt % active materials, 10 wt % acetylene black as conductive agent, and 5 wt % poly(tetrafluoroethylene) (PTFE) as binder to form a slurry, which was pressed onto a nickel foam. The electrodes were dried under vacuum at 60 °C for 12 h. Cyclic voltammetry (CV) test and galvanostatic charge-discharge (CD) test were carried out on a CHI660C electrochemistry workstation, and the electrochemical impedance spectroscopy (EIS) was carried on PARSTAT2273 workstation. The cycle performance of the active material was tested on Land 5.9 version workstation. All electrochemical measurements were finished in a three-compartment cell: a working electrode, a platinum plate as counter-electrode, and a Hg/HgO electrode as reference electrode. The electrolyte was 6 M KOH aqueous solutions.

Results and Discussion

Structural and Morphological Characterization. Figure 1 shows the XRD patterns of the prepared samples Co_3O_4, Co_3O_4/rmGO, Co_3O_4/moCNTs /rmGO. All diffraction peaks in Figure 1(a) can be indexed to face-centered cubic (fcc) Co_3O_4 phase (JCPDS card no. 43-1003).[43] No impurity phases were observed, demonstrating that the Co precursor was completely transformed into Co_3O_4 after hydrothermal reaction. Figure 1(b) displays the XRD pattern of Co_3O_4/rmGO. A broad peak appears at 24°, confirming the conversion of GO to graphene. The as-prepared Co_3O_4/moCNTs/rmGO composite was manifested in Figure 1(c). The peak due to graphene can also be identified. Besides, there were

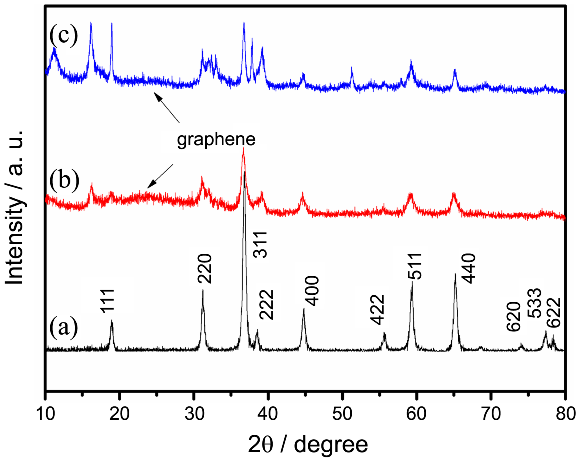

Figure 1. XRD pattern of Co_3O_4 (a), the product of Co_3O_4/rmGO (b), Co_3O_4/moCNTs /rmGO (c).

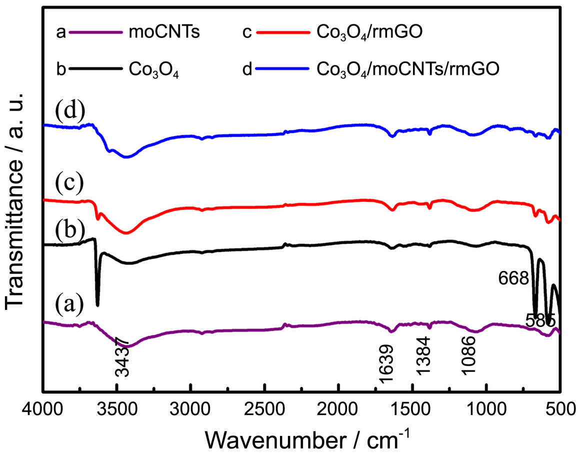

Figure 2. FT-IR spectra of moCNTs, Co_3O_4, Co_3O_4/rmGO, Co_3O_4/moCNTs/rmGO composite.

some peaks corresponding with the $Co(OH)_2$ phase (JCPDS card no. 30-0443), implying that the oxidation was incomplete to some extent.

The FT-IR spectra of the products are presented in Figure 2. The strong and sharp peaks at 668 and 583 cm^{-1} in Figure 2(b), 2(c), and 2(d) are attributed to the vibrations of the Co-O.[42] In Figure 2(b), peaks around 3,405 and 1,643 cm^{-1} are assigned to the stretching and bending vibration of water molecules, which is probably due to the absorbed moisture from the air during storage. No other impurities are detected, which indicates the formation of highly pure Co_3O_4. From Figure 2(a), a broad absorption band at 3,437 cm^{-1} is attributed to the hydroxyl group, which is due to water molecules and/or OH functional groups remaining even after reduction of CNT and GO.[45,46] The peak at 1,639 cm^{-1} is due to C=C stretching of the moCNTs and the peak at 1,384 cm^{-1} signifies the O-H bending deformation in -COOH. A small peak at 1,086 cm^{-1} is assigned to C-O bond stretching. Thus, the reminiscence of -OH and -COOH groups on moCNTs or rmGO due to functionalization is observed.

The shape of the Co_3O_4 nanoparticle on rmGO sheets was

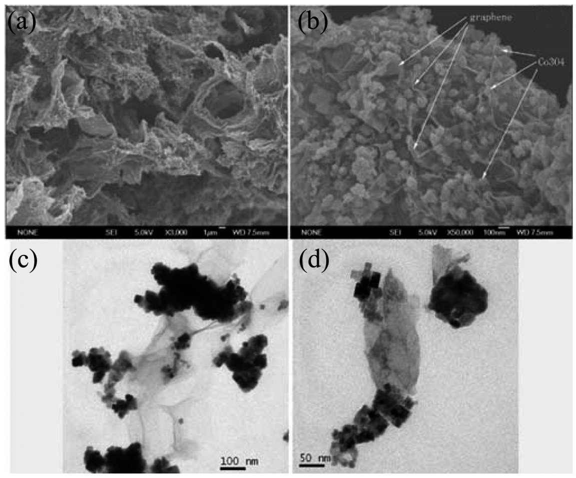

Figure 3. (a), (b) SEM image of Co_3O_4/rmGO and (c), (d) corresponding TEM images of Co_3O_4/rmGO after agitation for 1 h.

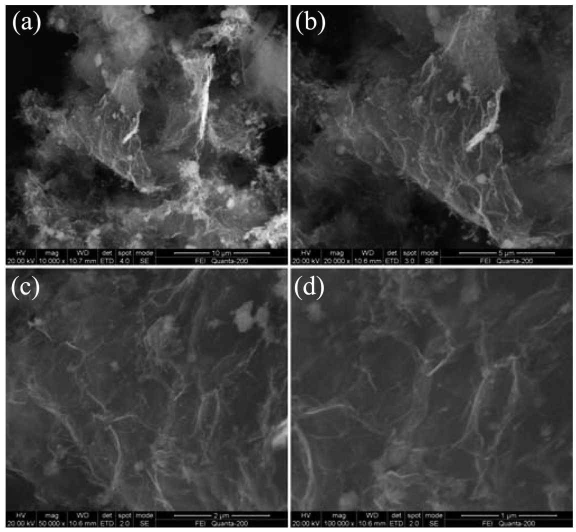

Figure 4. SEM images of Co_3O_4/moCNTs /rmGO.

confirmed by SEM images in Figure 3(a), (b) and the corresponding transmission electron microscope (TEM) image was also shown in Figure 3(c), (d). The folded graphene sheets with crumples wrapping the relatively uniform Co_3O_4 nanoparticles. In order to investigate the structural information of Co_3O_4/moCNTs/rmGO nanoparticle, TEM, high-resolution transmission electron microscopy (HRTEM) was investigated and presented in Figures 4 and Figure 5. The Co_3O_4/moCNTs/rmGO exhibits interconnected 3-D network in SEM image of different magnifications (Fig. 4(a), (b), (c), (d)). From Figure 5(a), it can be obviously observed that Co_3O_4 and moCNTs are scattered on the graphene sheets. The moCNTs are not found in Figure 5(b), and a few cobalt oxide nanoparticles were loosely decorated on the graphene nanosheet edge, resulting from the pretreatment of a strong ultrasonic. HRTEM image (Fig. 5(c)) shows a clear cubic lattice. The HRTEM image was recorded through the (111) direction. The (111) lattice spacing was 0.4777 nm. By using the formula for a cubic lattice: $a_0 = d(h^2 + k^2 + l^2)^{1/2}$, a_0 is

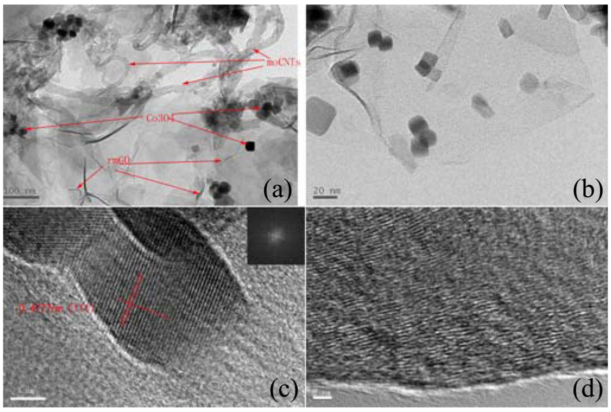

Figure 5. (a, b) TEM images of Co_3O_4/moCNTs/rmGO composites after agitation for 1 h; (c, d) HRTEM images of the Co_3O_4 nanoparticle surface and the moCNTs viewed from the broad plane. The inset in c shows the corresponding fast Fourier transform pattern.

calculated to be 0.808 nm, corresponding to the given value in the JCDS 43-1003 card.[47] Figure 5(d) shows the amorphous structure of moCNTs. On the basis of the nanostructural observations made from the above SEM and TEM images, the overall fabrication procedures of the Co_3O_4/moCNTs/rmGO composite are schematically[48] illustrated in Figure 6. The moCNTs that synthesized simply had introduced many carboxyl functional groups to imporve the dispersion stability and the functional groups on the outer walls to nucleate and anchor nanocrystals, while retaining intact inner walls for highly conducting network. Besides the moCNTs had negative charge in the surface, which was in favour of combination with Co ion. To some extent, the dispersed particles can effective alleviate the aggregation of rmGO. As a result, the composite had greatly improved in cyclability and rate capability.

The content of moCNTs and rmGO in Co_3O_4/moCNTs/rmGO was about 17.18% based on the weight loss before 700 °C in TGA (Fig. 7) for the decomposition of hydroxy group and the release of CO_2 from moCNTs and rmGO. The weight loss before 240 °C was attributed to the removal of

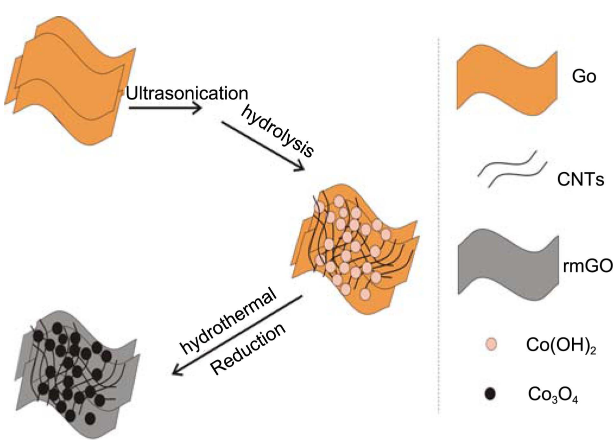

Figure 6. Schematic illustration for the synthesis of the Co_3O_4/moCNTs/rmGO composite.

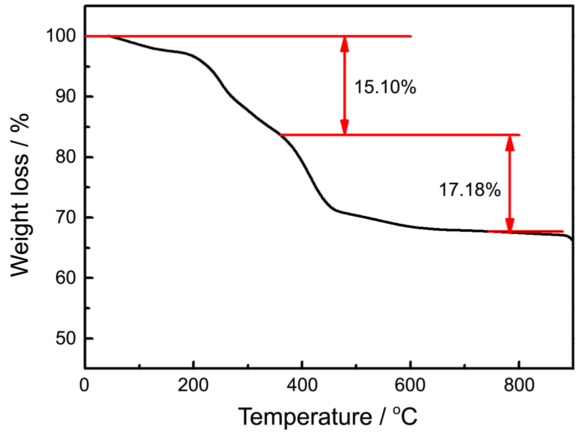

Figure 7. TGA curve of Co_3O_4/moCNTs/rmGO in air at 10 °C min^{-1}.

surface water.

Electrochemical Properties. The CV curves of Co_3O_4/moCNTs/rmGO composite at various scan rates of 5, 10 and 30 mV s^{-1} are displayed in Figure 8. There are a couple of redox peaks at about 0.351 and 0.485 V (*vs* Hg/HgO), indicating that pesudocapacitance originating from the electrochemically active Co_3O_4 component is dominant in the whole capacitance.[49] During the electron transfer procedure, only one oxidation peak can be clearly observed, possibly due to the production of CoOOH as an intermediate form which just existed for quite short time and then converted into CoO_2 rapidly. As the decreases of the scan rate, two oxidation peaks could appear, proving that CoOOH has relatively enough time to be detected in a given time scale, which can be changed into CoO_2. The peaks are related to the reactions between different oxidation states of Co according to the following equations:[50,51]

$$Co_3O_4 + H_2O + OH^- \rightleftharpoons 3CoOOH + e^- \quad (1)$$

$$CoOOH + OH^- \rightleftharpoons CoO_2 + H_2O + e^- \quad (2)$$

If the scan rate is increased, the anodic peaks shift toward

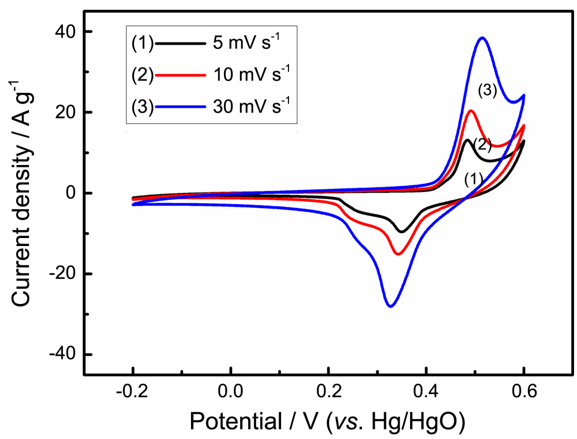

Figure 8. Cyclic voltammograms of Co_3O_4/moCNTs/rmGO electrode in 6 M KOH solution at various scan rates.

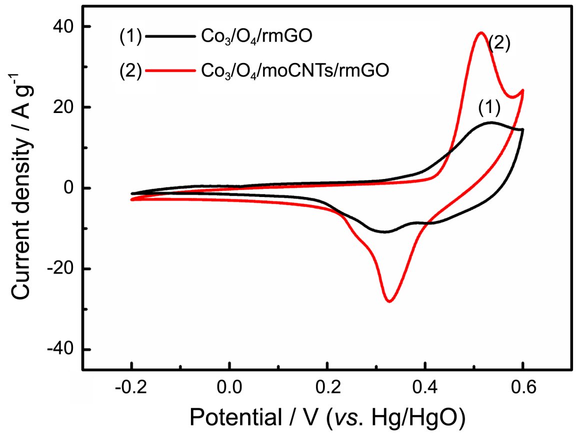

Figure 9. Cyclic voltammograms of Co_3O_4/rmGO, Co_3O_4/moCNTs/rmGO electrodes in 6 M KOH solution at a scan rate of 30 mV s^{-1}.

positive potential and the cathodic peaks move to negative potential. The potential difference between anodic and cathodic peaks is around 0.134 V at a scan rate of 10 mV s^{-1}, which indicates that the quasi-reversible feature of redox couples. The corresponding CV curves for Co_3O_4/rmGO and Co_3O_4/moCNTs/rmGO electrodes at 30 mV s^{-1} are displayed in Figure 9. The area of CV curve for Co_3O_4/moCNTs/rmGO is apparently larger than that of Co_3O_4/rmGO.

In addition, the rate performance of electrode materials is also crucial for supercapacitors. Galvanostatic charge-discharge curves of pure Co_3O_4 and Co_3O_4/moCNTs/rmGO composite are shown in Figure 10(a) and (b). It can be seen that the discharge curves consist of a sudden potential drop from 0.5 to 0.4 V and a slow potential decay from 0.4 to 0.3 V. It is in good agreement with CV results. The specific capacitance (SC), based on galvanostatic charge/discharge measurement, can be calculated from the following equation:

$$C = \frac{I \times \Delta t}{m \times \Delta V} \tag{3}$$

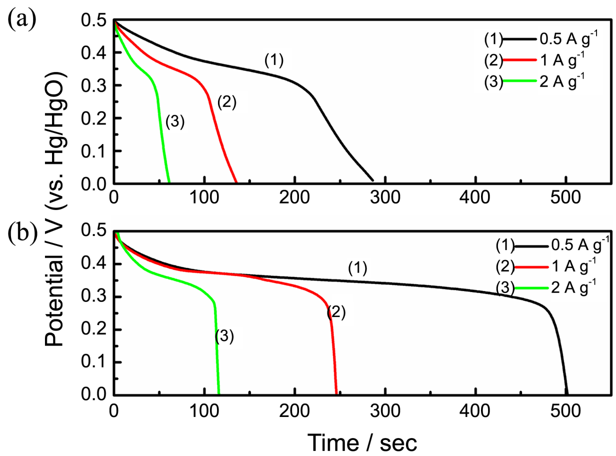

Figure 10. Galvanostatic discharge curves of pure Co_3O_4 (a) and Co_3O_4/moCNTs/rmGO composite (b) electrode in 6 M KOH solution at different current densities.

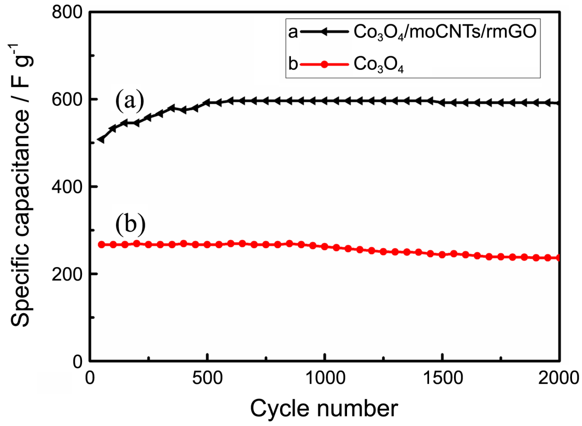

Figure 11. Cycling performances of Co_3O_4/moCNTs/rmGO composite and pure Co_3O_4 under a current density of 1 A g^{-1}.

where I is the discharge current (A), Δt is the discharge time (s), m is the mass of the electrode materials (g), and ΔV is the discharge potential range. In this paper, the voltage of galvanostatic charge-discharge tests are all ranging from 0 V to 0.5 V. Therefore, the value of specific capacitance for the Co_3O_4/moCNTs/rmGO composite is calculated to be 502, 492, 464 F g^{-1} at the current densities of 0.5, 1, 2 A g^{-1}, respectively. Compared to 286.3, 271.6, 245.2 F g^{-1} for pure Co_3O_4, the capacitance of the composite is remarkably enhanced and the utilization has doubled increasing from 8.04% to 16.85%, which is also higher than that surfactant-assisted synthesized Co_3O_4/reduced graphene oxide (163.8 F g^{-1}).[52] The higher specific capacitance of the Co_3O_4/moCNTs/rmGO composite than pure Co_3O_4 can be ascribed to the highly conductive network for electron transport, the better kinetic of electrode in the composite, and the ion transport channel between graphene and Co_3O_4 nanoparticles.

The long-term cycle stability of Co_3O_4/moCNTs/rmGO and pure Co_3O_4 electrodes were evaluated by repeating charge-discharge testing in 6 M KOH electrolyte at a current density of 1 A g^{-1} for 2,000 cycles. As shown in Figure 11, the specific capacitance of Co_3O_4/moCNTs/rmGO is increased

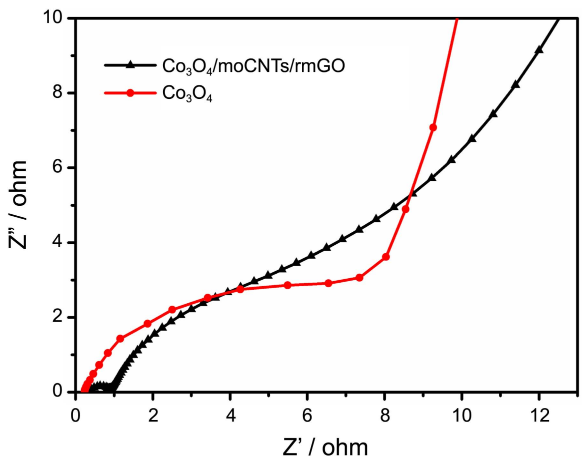

Figure 12. Nyquist plots for Co_3O_4/moCNTs/rmGO composite and pure Co_3O_4 eletrodes.

by 17% after 500 cycles, then remains almost at the same value during the following 1,500 cycles (Fig. 11(a)). In contrast, the pure Co_3O_4 presents a significant decrease in capacitance and just 88.6% of the initial capacitance can be maintained after 2000 cycles (Fig. 11(b)). The phenomenon could be attributed to the reasons as follows: at the initial cycle, the nanostructures wrapped by graphene have not been fully activated. After repeated charge-discharge cycling, the electrochemically active sites will be fully accessible by the electrolyte.

The EIS data of the pure Co_3O_4 and Co_3O_4/moCNTs/rmGO composites at open circuit potential are shown in Figure 12. It is found that Co_3O_4/moCNTs/rmGO shows a smaller radius of semicircle in the Nyquist plots as compared to Co_3O_4, suggesting that the Co_3O_4/moCNTs/rmGO possesses higher conductivity because of the presence of rmGO and moCNTs. These results indicate that the Co_3O_4/moCNTs/rmGO composites are suitable for fast charging and discharging. At very high frequency, the crossover point of the semicircle on the real part is a combinational resistance of the electrolyte resistance, intrinsic resistance of substrate, and contact resistance between the active materials and current collector. Meanwhile, it can be also found that charge-transfer resistance of pure Co_3O_4 is much larger than that of sample Co_3O_4/moCNTs/rmGO. Evidently, it indicates that the conductivity of sample Co_3O_4/moCNTs/rmGO is greatly improved in comparison with pure Co_3O_4, in good agreement with the all above discussion.

Conclusion

The rmGO plays as the base for the growth of moCNTs and Co_3O_4. The moCNTs and Co ion, to some extent, as the dispersed particles can effective alleviate the aggregation of rmGO. As a result, the composite exhibited greatly improved cyclability and rate capability. The composite had an outstanding conducting network structure and exhibited a high capacitance of 502 F g^{-1} in 6 M KOH electrolyte at 1 A g^{-1}, much higher than that of pure Co_3O_4. The rmGO and moCNTs also effectively restrain the volume expansion of Co_3O_4 during cycling and improve the conductivity of electrode, so the composite exhibits the excellent cycling performance without capacitance fading after 2000 cycles. The ternary composite is a promising candidate as the electrode for supercapacitors due to its high capacitance and excellent capacity retention. Taking the advantages of the new structure into consideration, we believe that the strategy could be readily applicable to other M_xO_y/moCNTs/rmGO (M=Fe, Co, Ni, Mn) composites.

Acknowledgments. We thank the National Natural Science Foundation of China (No. 21071153) for their financial support.

References

1. Arico, A. S.; Bruce, P.; Scrosati, B.; Tarascon, J. M.; Van Schalkwijk, W. *Nat. Mater.* **2005**, *4*, 366.
2. Maier, J. *Nat. Mater.* **2005**, *4*, 805.
3. Wu, Y.; Liu, S.; Wang, H.; Wang, X.; Zhang, X.; Jin, G. *Electrochim. Acta* **2013**, *90*, 210.
4. Robertson, A. D.; Armstrong, A. R.; Bruce, P. G. *Chem. Mater.* **2001**, *13*, 2380.
5. Li, H.; Balaya, P.; Maier, J. *J. Electrochem. Soc.* **2004**, *151*, A1878
6. Chen, J.; Xu, L. N.; Li, W. Y.; Gou, X. L. *Adv. Mater.* **2005**, *17*, 582.
7. Jamnik, J.; Maier, J. *J. Phys. Chem*. **2003**, *5*, 5215.
8. Chan, C. K.; Peng, H. L.; Liu, G.; McIlwrath, K.; Zhang, X. F.; Huggins, R. A.; Cui, Y. *Nat. Nanotechnol.* **2008**, *3*, 31.
9. Yamada, A.; Hosoya, M.; Chung, S. C.; Kudo, Y.; Hinokuma, K.; Liu, K. Y.; Nishi, Y. J. *Power Sources* **2003**, *119*, 232.
10. Fu, L. J.; Liu, H.; Li, C.; Wu, Y. P.; Rahm, E.; Holze, R.; Wu, H. Q. *Solid State Sci.* **2006**, *8*, 113.
11. Shi, W.; Zhu, J.; Sim, D. H.; Tay, Y. Y.; Lu, Z.; Zhang, X.; Sharma, Y.; Srinivasan, M.; Zhang, H.; Hng, H. H.; Yan, Q. J. *Mater. Chem.* **2011**, *21*, 3422.
12. Liu, C.; Yu, Z.; Neff, D.; Zhamu, A.; Jang, B. Z. *Nano Lett.* **2010**, *10*, 4863.
13. Geim, A. K.; Novoselov, K. S. *Nat. Mater.* **2007**, *6*, 183.
14. Du, X.; Skachko, I.; Barker, A.; Andrei, E. Y. *Nat. Nanotechnol.* **2008**, *3*, 491.
15. Balandin, A. A.; Ghosh, S.; Bao, W.; Calizo, I.; Teweldebrhan, D.; Miao, F.; Lau, C. N. *Nano Lett.* **2008**, *8*, 902.
16. Lee, C.; Wei, X.; Kysar, J. W.; Hone, J. *Science* **2008**, *321*, 385.
17. Stankovich, S.; Dikin, D. A.; Dommett, G. H. B.; Kohlhaas, K. M.; Zimney, E. J.; Stach, E. A.; Piner, R. D.; Nguyen, S. T.; Ruoff, R. S. *Nature* **2006**, *442*, 282.
18. Hu, C. C.; Chang, K. H.; Lin, M. C.; Wu, Y. T. *Nano Lett.* **2006**, *6*, 2690.
19. Dong, X. P.; Shen, W. H.; Gu, J. L.; Xiong, L. M.; Zhu, Y. F.; Li, Z.; Shi, J. L. *J. Phys. Chem. B* **2006**, *110*, 6015.
20. Yuan, C.; Su, L.; Gao, B.; Zhang, X. *Electrochim. Acta* **2008**, *53*, 7039.
21. Xiong, S.; Yuan, C.; Zhang, M.; Xi, B.; Qian, Y. *Chem-Eur. J.* **2009**, *15*, 5320.
22. Yuan, C.; Zhang, X.; Su, L.; Gao, B.; Shen, L. J. *Mater. Chem.* **2009**, *19*, 5772.
23. Choi, D.; Blomgren, G. E.; Kumta, P. N. *Adv. Mater.* **2006**, *18*, 1178.
24. Yuan, C.; Gao, B.; Su, L.; Chen, L.; Zhang, X. *J. Electrochem. Soc.* **2009**, *156*, A199.
25. Wang, Y. G.; Li, H. Q.; Xia, Y. Y. *Adv. Mater.* **2006**, *18*, 2619.
26. Zhang, K.; Zhang, L. L.; Zhao, X. S.; Wu, J. *Chem. Mater.* **2010**, *22*, 1392.
27. Mi, H.; Zhang, X.; An, S.; Ye, X.; Yang, S. *Electrochem. Commun.* **2007**, *9*, 2859.
28. Gao, B.; Fu, Q.; Su, L.; Yuan, C.; Zhang, X. *Electrochim. Acta* **2010**, *55*, 2311.
29. Mi, H.; Zhang, X.; Ye, X.; Yang, S. *J. Power Sources* **2008**, *176*, 403.
30. Soudan, P.; Lucas, P.; Ho, H. A.; Jobin, D.; Breau, L.; Belanger, D. *J. Mater. Chem.* **2001**, *11*, 773.
31. Pandolfo, A. G.; Hollenkamp, A. F. *J. Power Sources* **2006,** 157, 11.
32. Sarangapani, S.; Tilak, B.; Chen, C. P. *J. Electrochem. Soc.* **1996**, *143*, 3791.
33. Li, J.; Wang, X.; Huang, Q.; Gamboa, S.; Sebastian, P. J. *J. Power Sources* **2006**, *158*, 784.
34. Wu, Z. S.; Wang, D. W.; Ren, W.; Zhao, J.; Zhou, G.; Li, F.; Cheng, H. M. *Adv. Funct. Mater.* **2010**, *20*, 3595.
35. Yan, J.; Fan, Z.; Wei, T.; Qian, W.; Zhang, M.; Wei, F. *Carbon* **2010**, *48*, 3825.
36. Yu, G.; Hu, L.; Vosgueritchian, M.; Wang, H.; Xie, X.; McDonough, J. R.; Cui, X.; Cui, Y.; Bao, Z. *Nano Lett.* **2011**, *11*, 2905.

37. Meher, S. K.; Rao, G. R. *J. Phys. Chem. C* **2010**, *115*, 15646.
38. Zhang, X.; Sun, X.; Chen, Y.; Zhang, D.; Ma, Y. Ma, *Mater. Lett.* **2012**, *68*, 336.
39. Hwang, Y. H.; Bae, E. G.; Sohn, K. S.; Shim, S.; Song, X.; Lah, M. S.; Pyo, M. *J. Power Sources* **2013**, *240*, 683.
40. Prabakar, S. J.; Hwang, Y. H.; Bae, E. G.; Shim, S.; Kim, D.; Lah, M. S.; Sohn, K. S.; Pyo, M. *Adv. Mater.* **2013**, *25*, 3307.
41. Dai, H. J.; Liang, Y. Y.; Wang, H. L.; Diao, P.; Chang, W. *J. Am. Chem. Soc*. **2010**, 15849.
42. Liang, Y.; Li, Y.; Wang, H.; Zhou, J.; Wang, J.; Regier, T.; Dai, H. *Nat. Mater.* **2011**, *10*, 780.
43. Salavati-Niasari, M.; Fereshteh, Z.; Davar, F. *Polyhedron* **2009**, *28*, 1065.
44. Zhang, H.; Zhao, D.; Fu, Y. Y.; Han, Q. *J. Phys. Chem. C* **2007**, *111*, 18475.
45. Nina, I. K.; Thomas, E. M.; Ling, P., Elizabeth, C. D. *J. Am. Chem. Soc.* **2003**, *125*, 9761.
46. Eklund, P. C.; Kim, U. J.; Furtado, C. A.; Liu, X. M.; Chen, G. G. *J. Am. Chem. Soc.* **2005**, *127*, 15437.
47. Wang, N.; Guo, L.; He, L.; Cao, X.; Chen, C.; Wang, R.; Yang, S. *Small* **2007**, *3*, 606.
48. Shen, L.; Zhang, X.; Li, H.; Yuan, C.; Cao, G. *J. Phys. Chem. Lett.* **2011**, *2*, 3096.
49. Liang, Y.; Schwab, M. G.; Zhi, L.; Mugnaioli, E.; Kolb, U.; Feng, X.; Mullen, K. *J. Am. Chem. Soc.* **2010**, *132*, 15030.
50. Xue, T.; Wang, X.; Lee, J. M. *J. Power Sources* **2011**, *201*, 382.
51. Ko, J. M.; Soundarajan, D.; Park, J. H.; Yang, S. D.; Kim, S. W.; Kim, K. M.; Yu, K. H. *Curr. Appl. Phys.* **2012**, *12*, 341.
52. Zhou, W.; Zhu, J.; Cheng, C.; Liu, J.; Yang, H.; Cong, C.; Guan, C.; Jia, X.; Fan, H. J.; Yan, Q.; Li, C. M.; Yu, T. *Energ. Environ. Sci.* **2011**, *4*, 4954.